Current Switching Coupled to Molecular Spin-States in Large-Area Junctions

Constantin Lefter, Sylvain Rat, José Sánchez Costa, María Dolores Manrique-Juárez, Carlos M. Quintero, Lionel Salmon, Isabelle Séguy, Thierry Leichle, Liviu Nicu, Philippe Demont, et al.

Current Switching Coupled to Molecular Spin-States in Large-Area Junctions

Constantin Lefter, Sylvain Rat, José Sánchez Costa, María D. Manrique-Juárez, Carlos M. Quintero, Lionel Salmon, Isabelle Séguy, Thierry Leichle, Liviu Nicu, Philippe Demont, Aurelian Rotaru, Gábor Molnár,* and Azzedine Bousseksou**

Switchable molecular compounds are being more and more considered for the replacement of conventional inorganic semiconductor materials as the miniaturization of silicon based devices approaches fundamental technological and physical limits.[1] While early developments with molecular switches focused primarily on single molecule devices (a field referred to as "molecular electronics"),[2] the recent progress of "organic electronics"[3] and "organic spintronics"[4] has paved the way for considering the use of molecular switches in more conventional devices as well, such as field-effect transistors, light emitting diodes, spin valves, etc.

Transition metal complexes exhibiting spin crossover (SCO) phenomenon between the low spin (LS) and high spin (HS) electronic configurations[5–7] appear particularly attractive for the development of electronic and spintronic devices. Indeed, increasing interest has been focused recently on the charge transport properties of SCO compounds, including the investigation of the dielectric permittivity and electrical conductivity of bulk powders[8–10] and composite materials,[11–13] the integration of thin films,[14–17] nanoparticles,[18–21] and single molecules[22–28] into test devices. Here, we describe a novel approach for the investigation of the interplay between molecular spin-state switching and charge transport in SCO materials. Our approach is based on robust, well-reproducible, large-area vertical devices with nanomeric SCO spacer layers.

Obviously, the main bottleneck to our approach is the need for high quality, ultrathin, pinhole-free SCO films over large electrode areas, which resist also to the deposition of the upper metallic electrode. To this aim we have chosen the $[Fe(H_2B(pz)_2)_2(phen)]$ SCO complex **1** ($H_2B(pz)_2$ = dihydrobis(pyrazolyl)borate and phen = 1,10-phenanthroline, see **Figure 1**a),[29] which can be deposited on surfaces by thermal evaporation.[17,25,27,30–34]

The bulk powder of **1** displays a rather abrupt, cooperative, first-order thermal spin transition around 165 K with a very narrow hysteresis, while the vacuum-deposited films exhibit a very gradual (i.e., weakly cooperative) thermal spin crossover between ≈100 K (LS) and 200 K (HS). Both the powder and film samples are known to exhibit also light-induced excited spin-state trapping (LIESST) phenomenon with a long-lived metastable HS state below ≈50 K.[30] Interestingly, the spin crossover properties of the films are not much altered by the film thickness from the micrometer scale down to the isolated molecule level.[33,34] Previous X-ray diffraction studies revealed that the films are amorphous,[30] which explains probably the loss of the first-order nature of the spin transition (i.e. the lack of cooperativity), the lack of significant finite size effects as well as the remarkably smooth and homogenous film morphology observed even for very small thicknesses.

The schematic representation of the device made with **1** is shown in **Figure 2**a. The basic device architecture is fairly similar to the SCO devices reported by Matsuda et al.[14] Thin films of **1** were first grown by thermal evaporation on pre-patterned ITO (indium-tin-oxide) bottom electrodes on glass substrates. This choice of the substrate and the electrode was motivated by their optical transparency, which allows both for optical triggering and probing the spin-state changes in the devices using visible light irradiation. In the next step the upper Al electrodes were carefully deposited by thermal evaporation through a shadow mask into a crossbar configuration (Figure 2b). The effective junction area of each device is ≈3 mm^2. Junctions of **1** were fabricated in a single run with three different nominal thicknesses (10, 30, and 100 nm). The film thickness was monitored in situ during the deposition by a quartz crystal balance and was confirmed also ex situ by acquiring atomic force microscopy (AFM) data and scanning electron microscopy (SEM) images of the device tranches milled by focused ion beam (FIB) etching (Figure 2c—see also the Supporting Information.)

Dr. C. Lefter, S. Rat, Dr. J. Sánchez Costa,
M. D. Manrique-Juárez, Dr. C. M. Quintero,
Dr. L. Salmon, Dr. G. Molnár,
Dr. A. Bousseksou
LCC
CNRS and Université de Toulouse
UPS, INP
F-31077 Toulouse, France
E-mail: gabor.molnar@lcc-toulouse.fr;
azzedine.bousseksou@lcc-toulouse.fr

Dr. C. Lefter, Dr. A. Rotaru
Faculty of Electrical Engineering and Computer Science & MANSiD Research Center
Stefan cel Mare University
13, Str. Universitatii, Suceava 720229, Romania
E-mail: rotaru@eed.usv.ro

M. D. Manrique-Juárez, Dr. C. M. Quintero, Dr. I. Séguy, Dr. T. Leichle, Dr. L. Nicu
LAAS
CNRS & Université de Toulouse
INSA, UPS
F-31077 Toulouse, France

Prof. P. Demont
LPP-CIRIMAT
CNRS & Université de Toulouse III
31062 Toulouse, France

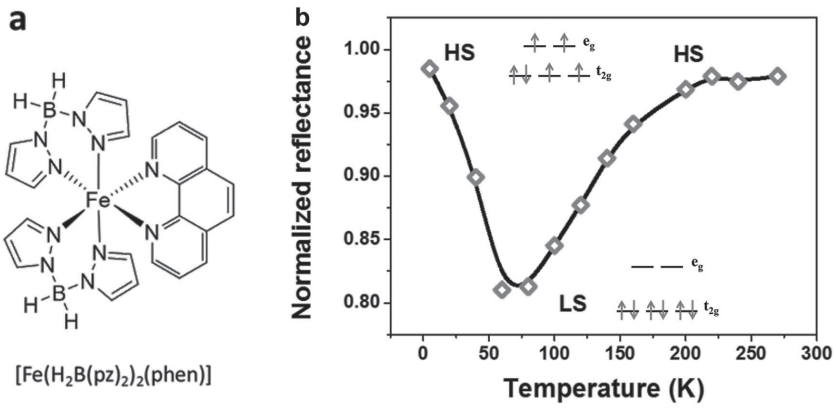

Figure 1. Structure and properties of the spin crossover compound **1.** a) Molecular structure of **1**. b) Variable temperature optical reflectance (λ = 640 nm) of a 100 nm thick film of **1** in an ITO/**1**/Al stack showing thermal (100–200 K) and photoinduced (<50 K) spin crossover phenomenon between the high spin and low spin states. The corresponding electronic configurations are also shown. The effective photoinduced population of the metastable HS state by the probe light is observed at low temperatures due to the very slow relaxation back to the ground LS state. The quantitative thermal population of the HS state at high temperatures is an entropy driven process.

AFM studies confirmed also the high quality of the films of **1** in terms of homogeneity and continuity (see Supporting Information). Of particular interest is the thinnest, nominally 10 nm film, for which AFM measurements revealed 8.5 nm thickness and 0.2 nm roughness, which was further confirmed by X-ray reflectometry (8.1 ± 0.2 nm) and by SEM (12 ± 3 nm). While the 10 nm films are smooth and continuous, for 5 nm thickness a few pinholes could be depicted hence no junctions of this size were fabricated. Since the spin transition in **1** is accompanied by a significant change in volume, the mechanical stress imposed by the "sandwich" geometry may change or even preclude the SCO in the device. To verify the occurrence of SCO we acquired optical reflectivity spectra of the glass/ITO/SCO (100 nm)/Al stack as a function of temperature between 300 and 5 K. This method probes the change in the refractive index associated with the spin transition.[35] As shown in Figure 1b the reflectance (λ = 640 nm) of the multilayer decreases significantly between ≈200 and 100 K and increases again to the initial level below 50 K. These changes of the reflectivity signal correspond, respectively, to the well-known thermal and photoinduced (LIESST effect) spin crossover in the films of **1**,[30–34] providing thus unambiguous evidence that the SCO properties are preserved in the sandwich structure. The photoinduced LS → HS SCO phenomenon was also detected in the 10 and 30 nm films through the refractive index changes, but due to the smaller thickness the measurement was carried out by depositing the films on a surface plasmon resonance sensor (see the Supporting Information for details). *I–V* characteristics of the different devices were strongly nonlinear and exhibited either temperature independent or insulating-like thermal activation behavior, which rules out the contribution of short circuit channels. These observations together with the highly reproducible device characteristics confirm the high

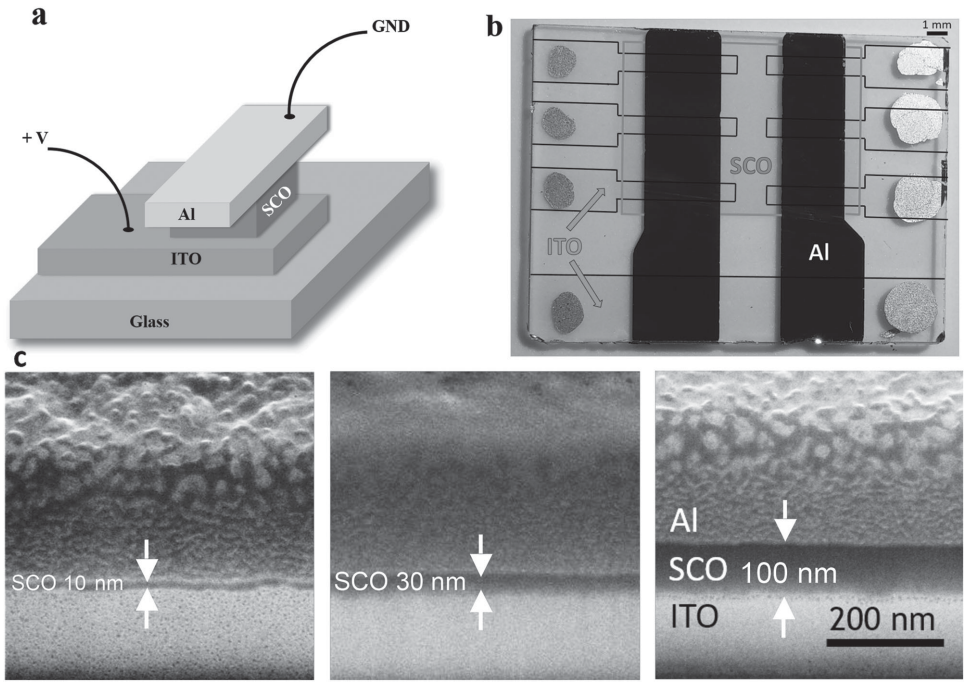

Figure 2. Device structure. a) Schematic representation of the ITO/SCO/Al junction. b) Photograph of a device with six crossbar junctions. The regions with ITO and SCO films are highlighted by black and grey lines, respectively. Silver paste contacts on the ITO are also visible. c) SEM images of FIB milled cross-sections of the junctions with different SCO film thickness (10, 30, and 100 nm).

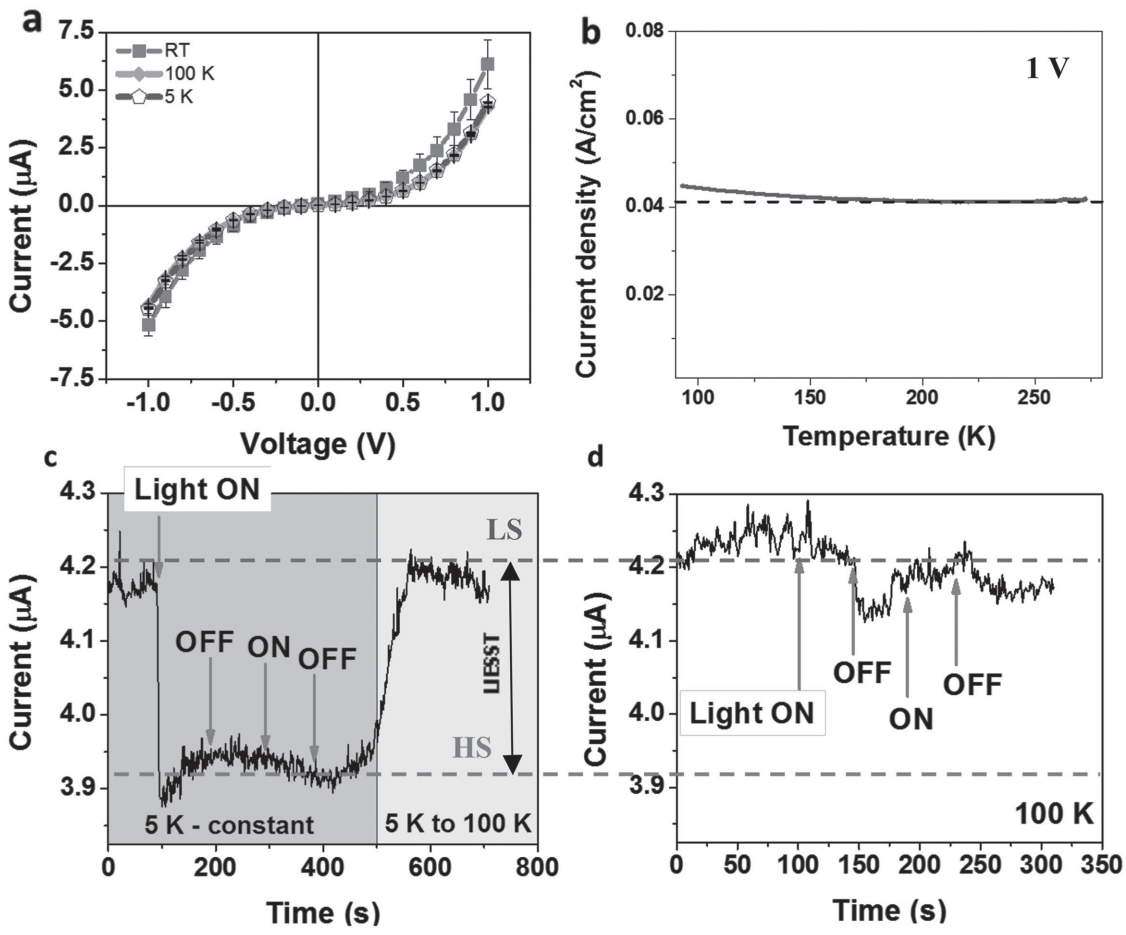

Figure 3. Electrical characteristics of a 10 nm junction. a) *I–V* curves registered at room temperature, 100 and 5 K at a rate of 100 mV s^{-1}. b) Temperature dependence of the current density in the junction registered at a rate of 5 K min^{-1}. c) Visible light irradiation effect on the current flowing in the junction at 5 K through two successive ON/OFF cycles (blue area), followed by heating from 5 to 100 K in the dark (yellow area). Current intensities in the HS and LS states are indicated by dashed lines. d) Visible light irradiation effect on the current flowing in the junction at 100 K through two successive ON/OFF cycles. The applied bias in (b–d) was 1 V.

quality of the SCO films in the junctions. The devices retained their characteristics during several tenths of thermal and bias cycles under electric fields up to ≈10^6 V cm^{-1} and could be stored in ambient air for several days reflecting thus high robustness. However, a slow increase of the junction resistances was also detected on a weekly time scale in air.

Variable temperature current–voltage curves registered for devices with 10 nm SCO layer (**Figure 3**a) are clearly characteristic of tunnel junctions. In particular, the thermal variation of the *I–V* curves is negligible in a broad temperature range (5–293 K), which is a generic feature of tunneling conduction. The *I–V* curves obey the relationship $I = I_0(V + \gamma V^3)$ and the differential conductance dI/dV curves exhibit parabolic shape typical of tunneling junctions[36] (see Supporting Information). A closer examination of the temperature dependence of the resistance of the junction at a constant bias of 1 V reveals a slight increase (≈10%) in the thermal spin crossover range between ≈200 and 100 K (Figure 3b). It is, however, impossible to conclude from these data on a link between the two phenomena because the reproducibility of the $I(T)$ data was comparable with the magnitude of the observed (small) changes.

In order to unambiguously demonstrate the influence of SCO on the device characteristics we used light irradiation to alter the spin-state of the junction. We cooled the device to 5 K in dark and we irradiated the sample using a halogen lamp. Immediately the current flowing in the device dropped by 7% from ≈4.2 to 3.9 μA ("Light ON" in Figure 3c). Following this first irradiation, the current intensity remained at the same level over successive irradiation cycles at 5 K (see OFF–ON–OFF in the blue area of Figure 3c) for more than one night. This finding can be obviously correlated with the LIESST effect: light irradiation leads to the population of the HS state, which is metastable at 5 K with a long lifetime of several days. To further substantiate the relationship between the current intensity and the spin state of the device this latter was heated to 100 K. As mentioned before, above ≈50 K the metastable HS state relaxes rapidly to the LS ground state. Indeed we observed that upon heating the current intensity rises back to the same level as before the first light irradiation (see yellow area in Figure 3c). This "dark cooling–photoswitching–heating" cycle was repeated three times with the same result. The device was also irradiated by light at 100 K where no LIEEST effect occurs, and in this case no significant effect

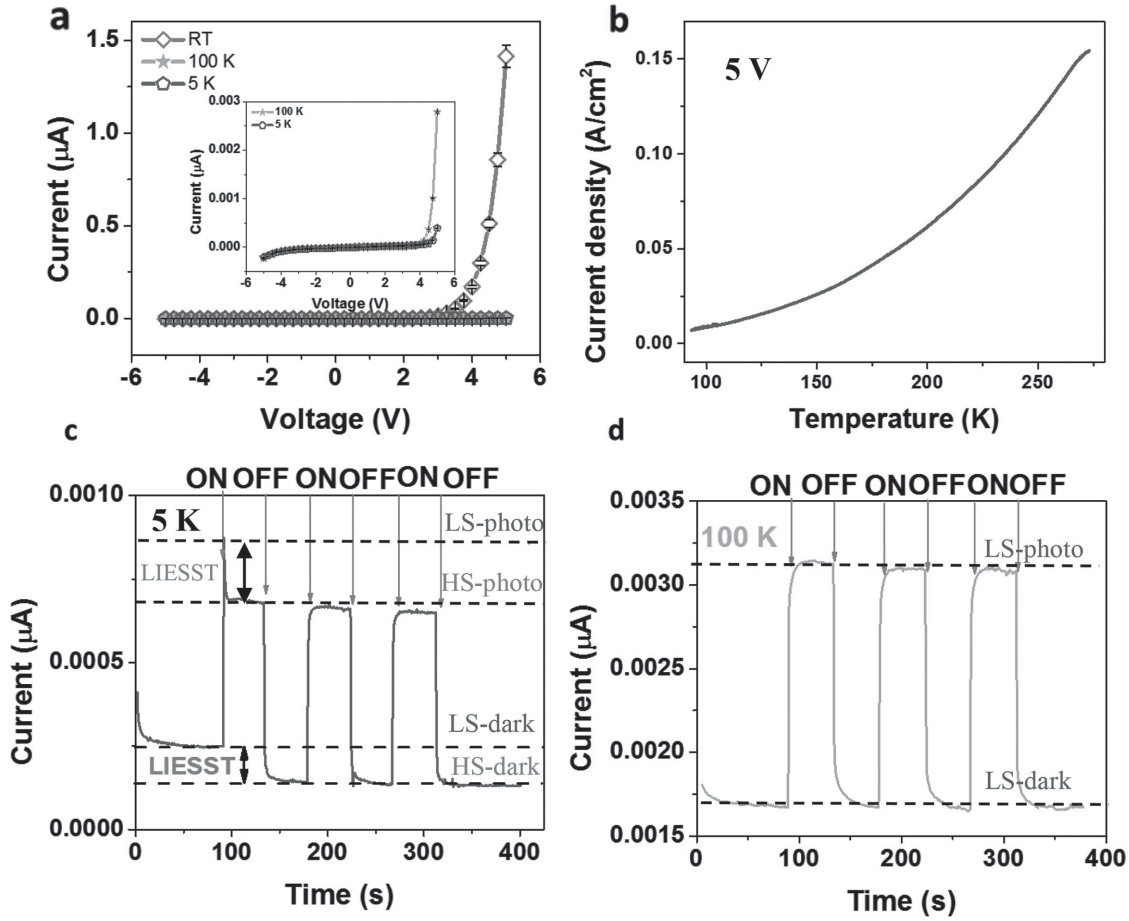

Figure 4. Electrical characteristics of a 30 nm junction. a) *I–V* curves registered at room temperature, 100 and 5 K at a rate of 100 mV s^{-1}. The inset is a zoom on the 100 and 5 K data. b) Temperature dependence of the conductivity of the junction registered at a rate of 5 K min^{-1}. c,d) Visible light irradiation effect on the current flowing in the junction through three successive ON/OFF cycles at 5 K (c) and 100 K (d). Current intensities in the HS and LS states are indicated by dashed lines both in dark and in photostationary conditions. The applied bias in (b–d) was 5 V.

on the conductivity was observed (Figure 3d). All these results point thus to the conclusion that switching the spin-state of the junction from the LS to the HS state leads to a well reproducible decrease of the tunneling current by 7%.

Figure 4 shows the characteristics of the 30 nm device. (Very similar results were obtained with 100 nm junctions, including also junctions with a poly(3,4-ethylenedioxythiophene):polystyrene-sulfonate (PEDOT:PSS) hole-transport layer, which are shown in the Supporting Information.) As it can be expected, the increasing junction width leads to a considerable change of the charge transport characteristics. The *I–V* curves display a rectifying behavior, with current flowing only under positive voltage, i.e., when the Al electrode is the cathode (Figure 4a). We fitted the *I–V* curves with the diode equation[37]

$$I = I_0\left[\exp\left(\frac{eV}{nk_BT}\right)-1\right]$$

where I_0 is the reverse bias current, k_B the Boltzmann constant, e the charge of electron and n the "nonideality" factor. While the fits are satisfactory down to 100 K, the fitted values of n are rather high (n = 12 at 293 K) when compared to the commonly observed ones (n = 1–2). This deviation from the usual behavior might be an indication of transport-limited current (vide infra). Even more important is the finding that the conductance of the 30 nm junction at a constant bias of 5 V is thermally activated—it increases by approximately one order of magnitude between 293 and 100 K (Figure 4b). The Arrhenius plot of the conductivity of the device exhibits a change of slope near 200 K in a reversible and reproducible manner. It is tempting to link this phenomenon with the occurrence of thermal SCO below 200 K, but this correlation may be only fortuitous. In this case also a more obvious correlation was obtained through light-induced spin-state switching experiments. When shining white light on the device at 5 K we observed a prompt increase of the current intensity from 250 to 872 pA, followed immediately by a decrease back to 687 pA (Figure 4c). When the light was turned off the current level dropped back to 145 pA. In the subsequent ON/OFF cycles we observed only a reversible switching between 145 and 665 pA. The complete sequence (dark cooling and light ON/OFF cycles) and associated photocurrent phenomena were well reproduced several times—in particular the characteristic "spike" upon the first irradiation was repeatedly detected.

In analogy with the 10 nm junction we assign the "irreversible" current drop during the first irradiation to the photoinduced spin-state trapping (LIESST) effect. One might notice that the LIESST effect in this junction is more important: when going from the LS to the HS state the current intensity drops by ≈50%. It is important to remark that at 100 K such "irreversible" photoeffect on the current was not observed in line with the fact that LIESST is not efficient at this temperature (Figure 4d). On the other hand, a significant "reversible" photocurrent was observed both at 5 and 100 K, the junction being approximately four times more conductive in the photostationary state with respect to the "dark" state. It is important to underline, however, that the spin-transition induced drop of the current intensity is not much different in the dark and photostationary cases. We suggest therefore that the "reversible" photocurrent probably originates from light absorption in the Al electrode near the interfacial layer. Since it was not observed in the 10 nm device we tentatively attribute this phenomenon to a photoactivated charge injection through the electrode interface barrier.

While a tunneling mechanism for the description of charge transport in the 10 nm junctions is obvious, for the thicker junctions the charge transport may be either injection-limited or bulk transport-limited. A common criterion used to identify the transport mechanism in low mobility semiconductor devices is based on the analysis of the current density on thickness for a given electric field.[38] In our devices a very strong dependence is observed (see Supporting Information), hence we conclude on a mostly bulk-limited mechanism, which is in line with the very low conductivity of **1**. This conclusion is also in agreement with the fact that the fit of the *I*–*V* curves by the diode equation gave physically meaningless results. To further investigate the charge transport process in the devices we have also acquired their dielectric spectra, i.e., the temperature and frequency *f* dependent complex permittivity ε^*. This latter can be related to the complex conductivity σ^* and dielectric modulus M^* by $\sigma^* = i\omega\varepsilon_0\varepsilon^*$, and $M^* = 1/\varepsilon^*$, respectively. (ε_0 is the permittivity of the free space and ω is the angular frequency.) **Figure 5** shows the frequency dependence of the real part of the complex conductivity σ' together with the dielectric loss modulus M'' acquired at selected temperatures for the 10 and 30 nm junctions. (See the Supporting Information for the 100 nm junction.) One can observe very similar frequency behavior between the different junctions. Each junction follows the Jonscher's power law of ac conductivity,[39] characteristic for hopping transport, $\sigma'(f) = \sigma_{ac}(f) = \sigma_{dc} + Af^s$, where σ_{dc} is the dc conductivity, *s* is the power law exponent and *A* is a constant. The frequency exponent *s* was found to be independent of both the temperature and the thickness of the junctions and takes a value of 1.82. A value of $s > 1$ means that charge carrier motion involves localized hopping between neighboring sites. In the electric modulus representation the frequency dependence of the loss modulus M'' reveals a simple Debye peak for each junction. This loss peak can be attributed to the conductivity relaxation process and the peak maxima is related to the relaxation time by $\tau_M = 1/\omega_{max} = \varepsilon_0\varepsilon_\infty/\sigma_{dc}$.[40] ($\varepsilon_\infty$ is the high frequency limit of ε'.) This relaxation times range between 10^{-4} and 10^{-2} s for the three junctions.

Based on these data the charge transport in the different devices can be ascribed to a similar short-range hopping conductivity process. The main difference between the dielectric spectra of the junctions is observed in their temperature dependence. In the case of the 30 and 100 nm junctions both the conductivity and the relaxation frequency exhibit thermal activation with a small activation barrier (see Supporting Information), while for the 10 nm junction both quantities are temperature independent. The weak temperature dependence implies that tunneling is important, particularly for the 10 nm junction. Taking into account the significant thickness of this latter junction tunneling must refer here to a multistep tunneling process by activationless hopping between localized states.[41–43] In the case of the 30 and 100 nm junctions the possible mechanism of the conduction can be described as a charge injection into the molecular orbitals (MOs) of **1** at one electrode interface (possibly by tunneling), followed by both diffusive tunneling and thermally activated hopping of charge carriers through the junction to the other interface, where the charge extraction occurs.

Starting from this picture of the charge transport in the different junctions we suggest that the spin-state dependence of the junction resistance is primarily related to the change of carrier hopping rates. It is well known that the hopping rate usually

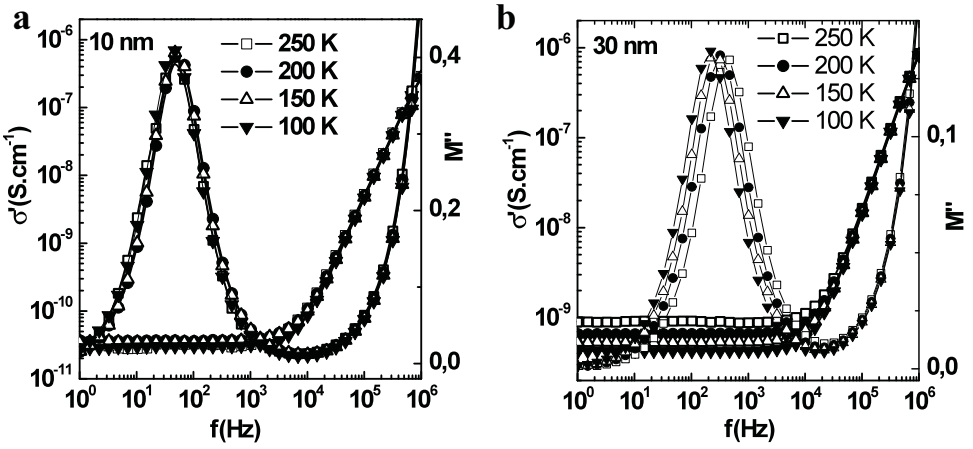

Figure 5. Frequency dependence of the real part of the ac conductivity and that of the loss modulus at selected temperatures for a 10 (a) and 30 nm (b) junction.

increases with increasing phonon frequencies and decreases with increasing distance between the localized states.[44] Since the LS to HS switching in **1** results in a significant increase of the metal-ligand distances and thus a decrease of the associated vibrational frequencies we understand that this switching process must lead to a lower current in the HS state, which is indeed observed in our experiments. Of course, a number of other parameters, such as the change of the dielectric permittivity and the thickness of the junction upon the SCO, will also impact the charge transport and will have to be analyzed in detail in future work. In any case it can be suggested that the current switching in our junctions is not a direct effect of the electronic state change, but it arises mostly due to the coupling of the electronic states with the crystal lattice (volume change) and in particular with the phonon density of states.

It is also instructive to compare the work functions of Al (4.2 eV) and ITO (4.5 eV) with the relevant molecular orbital energy levels of **1**. These latter were reported from density functional theory calculations by Gopakumar et al.[25] for a molecule of **1** adsorbed on Au(111) surface. They determined the HOMO/LUMO energy levels both in the HS (–3.5/–3.9 eV) and LS (–4.7/–2.6 eV) states (see Supporting Information). From cyclic voltammetry measurements (see Supporting Information) we inferred HOMO (–4.6 eV) and LUMO (–2.5 eV) energies in the LS state in good agreement with the theoretical data, but no HS data could be obtained for the lack of appropriate solvents. Nevertheless, it is obvious that the LS to HS switching must lead to a very significant decrease of the HOMO–LUMO gap. This picture would imply a substantial impact of the spin state switching on the injection barriers and thus on the current flowing in the device. This was not observed in our experiments, presumably due to the bulk-limited nature of the charge transport in our devices. Nevertheless, other phenomena at the electrode interfaces, such as the hybridization of molecular orbitals with substrate states at the electrode interface and subsequent loss of the SCO properties,[26] must be also considered. Hence an important perspective of our work will be the design of vertical SCO junctions with appropriate properties for injection-limited charge transport in which we expect a huge effect of SCO on the current intensity. This work will require the detailed study of different SCO and electrode materials with extensive interface engineering guided by MO calculations. Since the magnetic properties of the junction change also upon the SCO (diamagnetic vs paramagnetic) perhaps even more appealing prospects appear for spintronic applications. The technical challenge is substantial, however, as it will be necessary to develop methods for the deposition of pinhole-free films of these compounds between large area magnetic electrodes. Finally, taking into account the current state of the art of the SCO field[5–7] we can safely claim that there is no fundamental obstacle to prepare nanometric junctions with SCO compounds exhibiting near room temperature switching properties, which is of course very relevant for any technological application.

In summary, we fabricated vertical optoelectronic devices with thin films of the $[Fe(H_2B(pz)_2)_2(phen)]$ spin crossover complex sandwiched between large area electrodes. These devices allowed us to trigger and probe the spin-state switching in the SCO layer by optical means while detecting the associated electrical resistance changes in the junctions. The stable and high current intensity in the devices provided also possibility for mechanistic studies by means of temperature- and frequency-dependent dielectric spectroscopy. The devices with 10 nm junction width displayed activationless tunneling conductivity, while the thicker (30 and 100 nm) junctions exhibited diode-like rectifying characteristics and bulk-limited thermally activated currents. We provided experimental evidence that the spin-state switching of the junctions leads to a substantial and reversible increase/decrease of the current intensity (up to 50%) in the LS/HS states and we correlated this effect with the change of carrier hopping rates upon the spin conversion. Overall these results provide very promising novel perspectives for using spin crossover compounds in nanoelectronic and spintronic devices. To this aim it will be necessary to carry out more extensive investigations on a series of different SCO compounds with systematically modified MO levels and appropriate interface matching with different electrode materials.

Experimental Section

The bulk powder of complex **1** was synthetized using a procedure reported by Moliner et al.[29] with a small variation (see the Supporting Information for synthesis and characterization details). Thin films of **1** were grown by thermal evaporation at 110 °C in a high vacuum chamber (10^{-7} Torr) at a rate of 0.05 nm s^{-1} on 180 nm thick ITO electrodes. These latter were purchased from Praezisions Glas & Optik GmbH and patterned by wet etching using a conventional photolithography mask. Alternatively, for a 100 nm junction the surface of the ITO electrode was planarized by spin-coating a PEDOT:PSS hole transport layer on top of it. The upper 100 nm thick Al electrode was finally thermally evaporated through a shadow mask on the substrate. To avoid perforation of the SCO layer the Al film was deposited at a rate of 0.1 nm s^{-1} and the substrate was cooled by water. The films of **1** were characterized by AFM for their morphology and by optical methods to control the SCO properties (see Supporting Information for details). The junction widths were determined by SEM following FIB milling. *I–V* and *I–T* characteristics of the devices were acquired in two-probe mode using a Keithley-6430 source-meter and an Oxford Instruments OptistatCF liquid-helium cryostat. The device was irradiated by light through the cryostat windows using a 100 W halogen lamp. Dielectric spectra (1 Hz–1 MHz) of the devices and the powder sample were recorded between 100 and 250 K by means of a Novocontrol BDS 4000 broad-band dielectric spectrometer. Frequency sweeps were carried out isothermally and the applied AC voltage was 0.7 and 1 Vrms for the 10 and 30–100 nm junctions, respectively.

Supporting Information

Supporting Information is available from the Wiley Online Library or from the author.

Acknowledgements

This work was funded by the French RENATECH network and a joint ANR-UEFISCDI project (9RO-FR/01.02.2013, ANR-12-IS07-0003-01). C.L. thanks the French Ministry of Foreign Affairs for an Eiffel scholarship. S.R. thanks the French Education and Research Ministry for a MESR fellowship. M.D.M.-J. thanks the CONACYT for a PhD grant. J.S.C. thanks the IEF Marie-Curie research program (NanoSCOpe 328078).

[1] A. Aviram, M. A. Ratner, *Chem. Phys. Lett.* **1974**, *29*, 277.
[2] S. J. van der Molen, P. Liljeroth, *J. Phys.: Condens. Matter* **2010**, *22*, 133001.
[3] E. Orgiu, P. Samori, *Adv. Mater.* **2014**, *26*, 1827.
[4] D. Sun, E. Ehrenfreund, Z. V. Vardeny, *Chem. Commun.* **2014**, *50*, 1781.
[5] P. Gütlich, H. A. Goodwin, in *Spin Crossover in Transition Metal Compounds I* (Eds.: P. Gütlich, H. A. Goodwin), Springer, Berlin **2004**, pp. 1–47.
[6] A. Bousseksou, G. Molnár, L. Salmon, W. Nicolazzi, *Chem. Soc. Rev.* **2011**, *40*, 3313.
[7] P. Gütlich, A. Hauser, H. Spiering, *Angew. Chem. Int. Ed.* **1994**, *33*, 2024.
[8] A. Bousseksou, G. Molnár, P. Demont, J. Menegotto, *J. Mater. Chem.* **2003**, *13*, 2069.
[9] A. Rotaru, I. A. Gural'skiy, G. Molnar, L. Salmon, P. Demont, A. Bousseksou, *Chem. Commun.* **2012**, *48*, 4163.
[10] C. Lefter, I. A. Gural'skiy, H. Peng, G. Molnár, L. Salmon, A. Rotaru, A. Bousseksou, P. Demont, *Phys. Status Solidi RRL* **2014**, *8*, 191.
[11] Y.-S. Koo, J. R. Galán-Mascarós, *Adv. Mater.* **2014**, *26*, 6785.
[12] K. Takahashi, H. B. Cui, Y. Okano, H. Kobayashi, H. Mori, H. Tajima, Y. Einaga, O. Sato, *J. Am. Chem. Soc.* **2008**, *130*, 6688.
[13] H. Phan, S. M. Benjamin, E. Steven, J. S. Brooks, A. Shatruk, *Angew. Chem. Int. Ed.* **2015**, *54*, 823.
[14] M. Matsuda, H. Isozaki, H. Tajima, *Thin Solid Films* **2008**, *517*, 1465.
[15] T. Mahfoud, G. Molnár, S. Cobo, L. Salmon, C. Thibault, C. Vieu, P. Demont, A. Bousseksou, *Appl. Phys. Lett.* **2011**, *99*, 053307.
[16] S. Shi, G. Schmerber, J. Arabski, J.-B. Beaufrand, D. J. Kim, S. Boukari, M. Bowen, N. T. Kemp, N. Viart, G. Rogez, E. Beaurepaire, H. Aubriet, J. Petersen, C. Becker, D. Ruch, *Appl. Phys. Lett.* **2009**, *95*, 043303.
[17] X. Zhang, T. Palamarciuc, J.-F. Létard, P. Rosa, E. V. Lozada, F. Torres, L. G. Rosa, B. Doudin, P. A. Dowben, *Chem. Commun.* **2014**, *50*, 2255.
[18] F. Prins, M. Monrabal-Capilla, E. A. Osorio, E. Coronado, H. S. J. van der Zant, *Adv. Mater.* **2011**, *23*, 1545.
[19] C. Etrillard, V. Faramarzi, J.-F. Dayen, J.-F. Letard, B. Doudin, *Chem. Commun.* **2011**, *47*, 9663.
[20] A. Rotaru, J. Dugay, R. P. Tan, I. A. Guralskiy, L. Salmon, P. Demont, J. Carrey, G. Molnár, M. Respaud, A. Bousseksou, *Adv. Mater.* **2013**, *25*, 1745.
[21] J. Dugay, M. Giménez-Marqués, T. Kozlova, H. W. Zandbergen, E. Coronado, H. S. J. van der Zant, *Adv. Mater.* **2015**, *27*, 1288.
[22] V. Meded, A. Bagrets, K. Fink, R. Chandrasekar, M. Ruben, F. Evers, A. Bernand-Mantel, J. S. Seldenthuis, A. Beukman, H. S. J. van der Zant, *Phys. Rev. B* **2011**, *83*, 245415.
[23] G. D. Harzmann, R. Frisenda, H. S. J. van der Zant, M. Mayor, *Angew. Chem. Int. Ed.* **2015**, *54*, 13425.
[24] E. J. Devid, P. N. Martinho, M. V. Kamalakar, I. Šalitroš, Ú. Prendergast, J.-F. Dayen, V. Meded, T. Lemma, R. González-Prieto, F. Evers, T. E. Keyes, M. Ruben, B. Doudin, S. J. van der Molen, *ACS Nano* **2015**, *9*, 4496.
[25] T. G. Gopakumar, F. Matino, H. Naggert, A. Bannwarth, F. Tuczek, R. Berndt, *Angew. Chem. Int. Ed.* **2012**, *51*, 6262.
[26] T. Miyamachi, M. Gruber, V. Davesne, M. Bowen, S. Boukari, L. Joly, F. Scheurer, G. Rogez, T. K. Yamada, P. Ohresser, E. Beaurepaire, W. Wulfhekel, *Nat. Commun.* **2012**, *3*, 938.
[27] A. Pronschinske, Y. Chen, G. F. Lewis, D. A. Shultz, A. Calzolari, N. Buongiorno Nardelli, D. B. Dougherty, *Nano Lett.* **2013**, *13*, 1429.
[28] M. S. Alam, M. Stocker, K. Gieb, P. Müller, M. Haryono, K. Student, A. Grohmann, *Angew. Chem. Int. Ed.* **2010**, *49*, 1159.
[29] N. Moliner, L. Salmon, L. Capes, M. C. Muñoz, J.-F. Létard, A. Bousseksou, J.-P. Tuchagues, J. J. McGarvey, A. C. Dennis, M. Castro, R. Burriel, J. A. Real, *J. Phys. Chem. B* **2002**, *106*, 4276.
[30] T. Palamarciuc, J. C. Oberg, F. E. Hallak, C. F. Hirjibehedin, M. Serri, S. Heutz, J.-F. Létard, P. Rosa, *J. Mater. Chem.* **2012**, *22*, 9690.
[31] H. Naggert, A. Bannwarth, S. Chemnitz, T. von Hofe, E. Quandt, F. Tuczek, *Dalton Trans.* **2011**, *40*, 6364.
[32] H. Naggert, J. Rudnik, L. Kipgen, M. Bernien, F. Nickel, L. M. Arruda, W. Kuch, C. Nather, F. Tuczek, *J. Mater. Chem. C* **2015**, *3*, 7870.
[33] B. Warner, J. C. Oberg, T. G. Gill, F. El Hallak, C. F. Hirjibehedin, M. Serri, S. Heutz, M.-A. Arrio, P. Sainctavit, M. Mannini, G. Poneti, R. Sessoli, P. Rosa, *J. Phys. Chem. Lett.* **2013**, *4*, 1546.
[34] M. Bernien, H. Naggert, L. M. Arruda, L. Kipgen, F. Nickel, J. Miguel, C. F. Hermanns, A. Krger, D. Krger, E. Schierle, E. Weschke, F. Tuczek, W. Kuch, *ACS Nano* **2015**, *9*, 8960.
[35] I. A. Gural'skiy, C. M. Quintero, K. Abdul-Kader, M. Lopes, C. Bartual-Murgui, L. Salmon, P. Zhao, G. Molnar, D. Astruc, A. Bousseksou, *J. Nanophotonics* **2012**, *6*, 063517.
[36] J. G. Simmons, *J. Appl. Phys.* **1963**, *34*, 1793.
[37] R. K. Gupta, R. A. Singh, *J. Polym. Res.* **2005**, *11*, 269.
[38] M. A. Baldo, S. R. Forrest, *Phys. Rev. B* **2001**, *64*, 085201.
[39] A. K. Jonscher, *Nature* **1977**, *267*, 673.
[40] G. Molnar, S. Cobo, T. Mahfoud, E. J. M. Vertelman, P. J. van Koningsbruggen, P. Demont, A. Bousseksou, *J. Phys. Chem. C* **2009**, *113*, 2586.
[41] M. Gobbi, F. Golmar, R. Llopis, F. Casanova, L. E. Hueso, *Adv. Mater.* **2011**, *23*, 1609.
[42] P. Dey, R. Rawat, S. R. Potdar, R. J. Choudhary, A. Banerjee, *J. Appl. Phys.* **2014**, *115*, 17C110.
[43] T. L. A. Tran, T. Q. Le, J. G. M. Sanderink, W. G. van der Wiel, M. P. de Jong, *Adv. Funct. Mater.* **2012**, *22*, 1180.
[44] N. F. Mott, *Phil. Mag.* **1969**, *19*, 835.